Russian Chemical Reviews **83** (4) 365 – 375 (2014) © 2014 Russian Academy of Sciences and Turpion Ltd

DOI 10.1070/RC2014v083n04ABEH004405

Thermal stability of consolidated metallic nanomaterials

R A Andrievski

Institute of Problems of Chemical Physics, Russian Academy of Sciences
prosp. Akademika Semenova 1, 142432 Chernogolovka, Moscow Region, Russian Federation

The results of applications of theoretical kinetic and thermodynamic approaches to estimation of thermal stability of consolidated nanomaterials based on various metals, alloys and refractory compounds are considered. The principal experimental data concerning the stability of the nanomaterials, including radiation stability, abnormal grain growth and oxidation, are analyzed.
The bibliography includes 82 references.

Contents

I. Introduction 365
II. Theoretical approaches and modelling of thermal stability 365
III. Experimental studies of high-temperature behaviour of nanomaterials 369
IV. Conclusion 374

I. Introduction

The problem of stability of structure and properties of nanomaterials is one of the most important in modern material science.[1] Undoubtedly, the existence of numerous interfaces, segregations, residual stresses, nano- and micropores and non-equilibrium phases in nanomaterials results in excess free energy, while thermal, strain, radiation and some other impacts stimulate recrystallization, relaxation and homogenization (or segregation) processes leading to changes in nanostructures (up to their degradation) accompanied by deterioration of their physicochemical and mechanical properties. A consequence of the general technological progress is the increase in the temperature and duration of operation of devices applied in chemical machine industry and aicraft, missile and nuclear technology. In this context, enhancement of the stability of nanostructures acquires great importance for both fundamental and applied research preceding the development of methods for prediction of reliability of nanomaterials and the cost efficiency of their use.

Analysis of the regularities of thermal stability of nanomaterials based on the data obtained before 2002 was carried out in an earlier review.[2] The data on thermal stability of nanomaterials published up to 2010 were also surveyed.[1, 3, 4] The information in this area is rapidly accumulated, a few tens of studies being published over the past 2 – 3 years. Therefore, it is reasonable to return to analysis of the data, the more so because the problems of radiation stability and specific features in the interaction of nanomaterials with corrosive media have already been considered.[5, 6]

The general problem of the thermal stability of nanostructures is rather broad, it includes different aspects of behaviour of both single nanoparticles and consolidated nanomaterials, *e.g.*, the influence of temperature on the size and shape of nanograins, the aggregation processes in the case of nanoporous and nanopowdered objects, interactions with the environment and radiation fields, catalytic and sorption activity, diffusion redistribution of components, phase transitions, *etc*. Due to diversity of nanomaterials, exhaustive consideration of these issues is beyond the scope of a usual review; therefore, the present discussion is mainly focused on the analysis of the role of thermal and temporal factors, as well as on possible influence of radiation and oxidative processes on the changes in nanostructure of consolidated (predominantly metallic) nanomaterials.

II. Theoretical approaches and modelling of thermal stability

The driving force of grain growth is the decrease in the Gibbs free energy (ΔG) of grain boundaries with a decrease in their area. Grain growth in nanomaterials is a result of translation (migration) or rotation and merging (Fig. 1). The rotation mechanism has been studied to a lesser extent; therefore, it is necessary to dwell shortly on several studies devoted to its specific features in nanomaterials. Using molecular dynamics simulation, it was shown[7] that both mechanisms of grain growth can operate simultaneously in nanostructures, the rate of grain rotation and its contribu-

R A Andrievski Doctor of Technical Sciences, chief researcher of the group of Nanostructured Materials at the IPCP RAS.
Tel. (7-496) 522 77 93, e-mail: ara@icp.ac.ru
Current research interests: nanostructured materials science, solid-state physics and chemistry, interstitial phases (hydrides, carbides, nitrides and borides).

Received 7 May 2013
Uspekhi Khimii **83** (4) 365 – 375 (2014); translated by S E Boganov

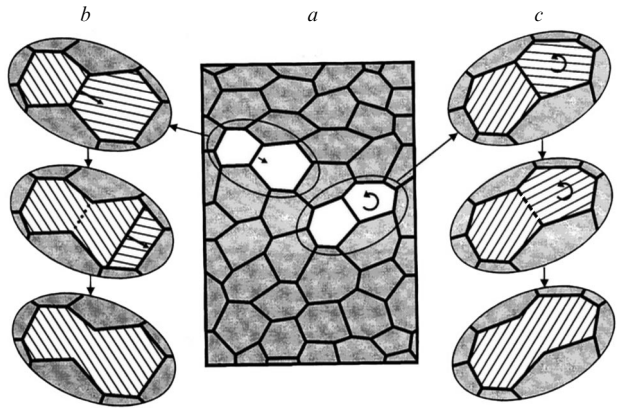


Figure 1. Grain growth mechanisms.[3]
(*a*) General view of the initial state; (*b*) migration and merging; (*c*) rotation and merging.

tion to the overall growth in comparison with the rate and contribution of gran migration increasing with decreasing size of the grains. Bernstein [8] paid attention to the dependence of rotation rate on the geometry of adjacent grains. Using yttrium oxide as an example, it was shown [9] that low-energy small-angle boundaries are formed upon rotation of grains of 20 and 200 nm in size at 600–1000 °C. There is an interesting observation of collective grain rotation upon irradiation of nanocrystalline Ti, TiN and NiO layers with a high-energy (E = 350 MeV) beam of gold ions.[10]

Nanograin growth and, hence, the degradation of nanostructures in consolidated nanomaterials can be inhibited by pores and phase inclusions upon changes in the initial grain size and decrease in their mobility owing to doping (including formation of segregations at grain boundaries) and spinodal decomposition. The speed of movement (v) of the grain boundary is usually described by the following equation

$$v = MP = M_0 \exp\left(\frac{-Q_\mathrm{m}}{RT}\right)\frac{2\gamma_\mathrm{g}}{r_\mathrm{g}} \qquad (1)$$

where M is the grain mobility, P is the driving force, M_0 is a pre-exponential factor, Q_m is the activation energy of boundary movement, γ_g is the grain boundary energy, and r_g is the radius of curvature of the grain.

There are roughly two approaches to the description of grain growth inhibition — kinetic (due to decreasing mobility) and thermodynamic ones (due to reduction of the driving force owing to decrease in the grain boundary energy). The theoretical descriptions of these approaches have been developed to different extents, although the grain growth inhibition by inclusions has been known for a long time and finds wide application in practice. Restraining the grain growth by nanoinclusions (so-called Zener pinning) is described by the formula

$$P_\mathrm{Z} = \frac{3V_r\gamma_i}{2r_i} \qquad (2)$$

where P_Z is the Zener drag force, which is the inhibiting force per unit boundary area, V_r is the volume fraction of inclusions with radius r_i, γ_i is the interfacial surface energy of inclusions.

As can be seen from Eqn (2), efficient retardation of grain growth can be achieved by increasing the volume fraction of inclusions and decreasing their radii.

In a series of studies of Novikov and co-workers and Shwindlerman and co-workers,[11–15] the influence of nanoinclusions, pores, triple and quadruple intergrain junctions on the thermal evolution of the material structure was analyzed in the framework of kinetic approach, taking into account the grain size. In particular, it was found that the stronger grain growth inhibition by triple and quadruple junctions is observed for initially smaller grains.[11] This effect is especially pronounced at moderate temperatures, while at higher temperatures, inversion of this regularity takes place, and the boundaries with junctions become more mobile. With the use of thermodynamic analysis, the value and sign of line tension of triple junctions were determined [the triple line tension was found to be $(6.0 \pm 3.0) \times 10^{-9}$ J m^{-1}].[12] The obtained value made it possible to correct the magnitude of the driving force of grain growth. Assuming that γ_g = 0.6 J m^{-2} for copper, the critical value of the average grain size below which the role of triple junctions must be taken into account in estimation of boundary migration is ~55 nm.

The dual nature of nanostructure evolution was revealed in numerical simulations of the movement of nanoparticles during grain boundary migrations, in particular, depending on the volume fraction of nanoparticles and overall velocity of boundary migration, the mobility of the boundaries not only can decrease but also can increase, resulting in abnormal grain growth.[13, 14] The analysis of possible interactions between pores and grains showed that the grain growth and disappearance of pores during annealing can follow different kinetic laws depending on their size and mobility.[15]

As for analysis of the decrease in grain boundary mobility in the framework of the thermodynamic approach, most important appear the studies on development of thermodynamics of binary nanosystems (so-called nanothermodynamics) which propose methods for estimation of the Gibbs free energy of alloys considering not only concentration factor but also the presence of nanograins (see, *e.g.*, Refs 16–19). The key point of these studies consists in the use of conventional regular solution approximation [20] for both intergrain (segregation) gaps and internal parts of nanograins (Fig. 2). Having omitted the intermediate mathematics, one can write the expression for the total ΔG value:[17, 18]

$$\Delta G = (1-f_\mathrm{b})\Delta G_\mathrm{g} + f_\mathrm{b}\Delta G_\mathrm{b} + z\psi f_\mathrm{b}(X_\mathrm{b} - X_\mathrm{g})\left[(2X-1)\omega_\mathrm{b} - \frac{\Omega^\mathrm{B}\gamma_\mathrm{g}^\mathrm{B} - \Omega^\mathrm{A}\gamma_\mathrm{g}^\mathrm{A}}{zt}\right] \qquad (3)$$

where f_b is the volume fraction of intergrain gaps

$$f_\mathrm{b} = 1 - \left(\frac{d-t}{d}\right)^3$$

d is the grain size, ΔG_g and ΔG_b are Gibbs free energies for grain internal space and intergrain gaps, respectively, z is the coordination number for the bulk material; ψ is the fraction of atoms having interatomic bonds in intergrain gaps; X_b and X_g are concentrations of the additive in

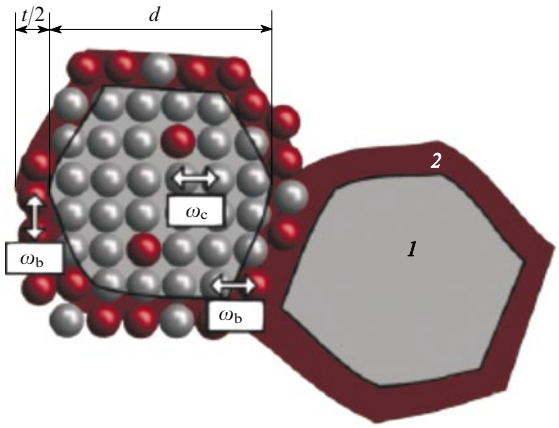


Figure 2. Schematic representation of two nanograins of size d and intergrain gap of width t. Grey and red spheres correspond to atoms of the solvent and the dissolved element, respectively.[18] (*1*) Internal space of the grain, (*2*) intergrain gap; ω_c and ω_b are the interaction parameters for regions *1* and *2*.

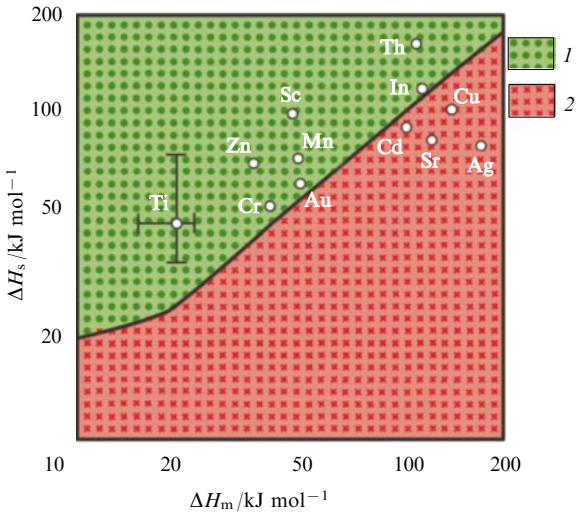


Figure 4. Stability map for tungsten-based alloys at 1100 °C.[17] (*1*) The region of existence of nanocrystalline alloys; (*2*) the region of existence of coarse-grained alloys.

intergrain gaps and internal space, which satisfy the following relation for the mean concentration

$$X = f_b X_b + (1 - f_b) X_g$$

ω_b is a parameter of interaction in intergrain gap, which is determined in the theory of regular solutions *via* the pair interaction energies

$$\omega = E^{AB} - \frac{E^{AA} + E^{BB}}{2}$$

t is the width of an intergrain gap, which is usually taken to be 0.5–1 nm; Ω^A and Ω^B are the atomic volumes of components of the alloy A + B (B is additive); γ_g^A and γ_g^B are the specific energies of grain boundaries of the A and B components.

The ΔG value is calculated by varying the d values and thermodynamic properties of different compositions; this allows one to determine characteristics of the most stable nanoalloys. As an example, the dependence of ΔG on the grain size and the concentrations of an additive in the intergrain gap is shown in Fig. 3. As can be seen, the ΔG minimum at the given values of overall concentration X,

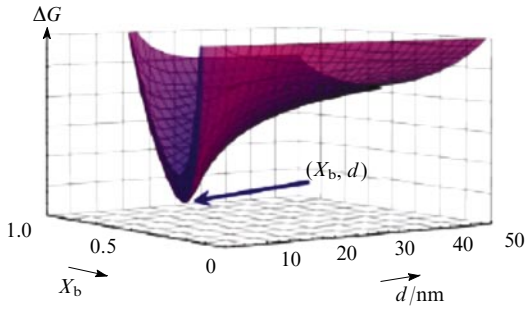


Figure 3. Gibbs free energy, ΔG, *vs.* grain size and concentration of an additive in the intergrain gap X_b.[18]

temperature T and interaction factor ω_b corresponds to the alloy with a grain size of ~25 nm and almost complete segregation of one of the components at grain boundaries.

Various situations of ΔG minimization as applied to the grain growth and phase decomposition (composition variations, changes in temperature and interaction parameters, the absence of ΔG minimum, various combinations of enthalpies of mixing and segregation, formation of amorphous interlayers in intergrain gaps, existence of metastable nanoalloys, formation of two-phase nanocomposites, *etc.*) were analyzed in detail.[18]

The dependence of segregation enthalpy (ΔH_s) on the mixing enthalpy (ΔH_m) for various tungsten alloys at 1100 °C is given in Fig. 4. The nanocrystalline state is observed for alloys which correspond to the points located above the plot $\Delta H_s = f(\Delta H_m)$; the points corresponding to coarse-grained alloys are below the plot (region *2*).

The segregation and mixing enthalpies were calculated from the following formulae:

$$\Delta H_s = z\left(\omega_g - 0.5\omega_b - \frac{\Omega^B \gamma_g^B - \Omega^A \gamma_g^A}{2zt}\right)$$

and

$$\Delta H_m = z\omega_g X(1-X)$$

A similar approach based on the regular solution approximation for regions *1* and *2* (see Fig. 2) was developed in another study,[19] in which the temperature effect on the size of nanograins and segregations in the intergrain gaps was estimated for Fe–Zr, Cu–Zr, Cu–Nb and Ni–W alloys depending on the concentration of the second component. Some initial data for these calculations are given in Table 1. In addition to the purely chemical interaction, the contribution of the elastic interaction during alloy formation was taken into account [19] in the calculations of ΔG, the grain boundary energy was assumed to be 1/3 of the surface energy. The temperature dependences of grain growth for different alloy concentrations given in Table 1 are shown in Fig. 5. Analysis of the data showed that the

Table 1. Input data for the calculation of thermal stability of some alloys.[19]

Parameter	Fe–Zr	Cu–Zr	Cu–Nb	Ni–W
Concentration range for the second component (at.%)	2–8	4–7	1–5	5–25
Coordination number z	8	12	12	12
Grain boundary energy of the solvent metal γ^A /J m^{-2}	0.805	0.602	0.602	0.793
Grain boundary energy of the dissolved metal γ^B /J m^{-2}	0.636	0.636	0.885	1.088
Enthalpy of elastic interaction ΔH_e /kJ mol^{-1}	−109.3	−90.8	−40.2	−44.4
Mixing enthalpy ΔH_m /kJ mol^{-1}	−25	−23	−3	−3

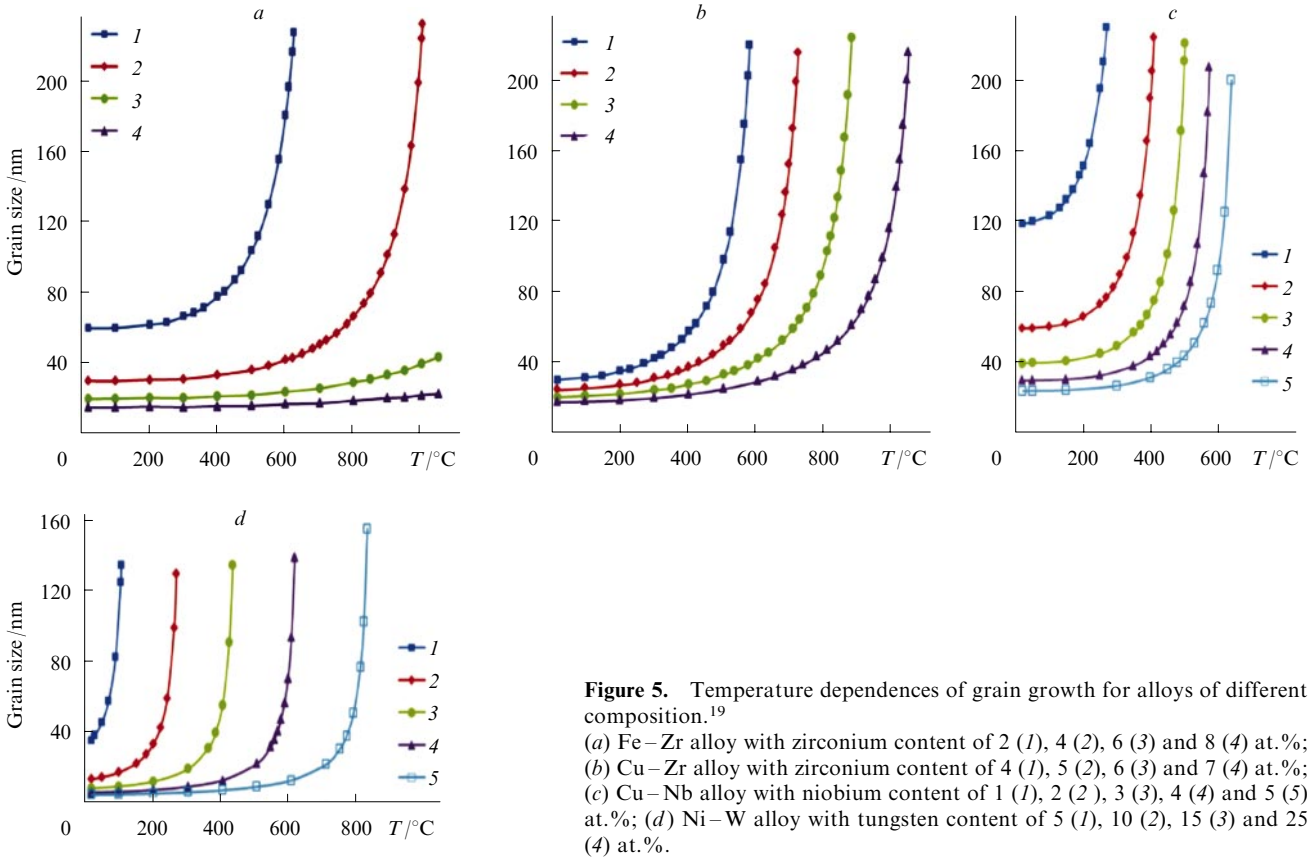


Figure 5. Temperature dependences of grain growth for alloys of different composition.[19]
(*a*) Fe–Zr alloy with zirconium content of 2 (*1*), 4 (*2*), 6 (*3*) and 8 (*4*) at.%; (*b*) Cu–Zr alloy with zirconium content of 4 (*1*), 5 (*2*), 6 (*3*) and 7 (*4*) at.%; (*c*) Cu–Nb alloy with niobium content of 1 (*1*), 2 (*2*), 3 (*3*), 4 (*4*) and 5 (*5*) at.%; (*d*) Ni–W alloy with tungsten content of 5 (*1*), 10 (*2*), 15 (*3*) and 25 (*4*) at.%.

strongest decrease in the grain growth upon annealing of nanoalloys was observed for iron with a minor amount of zirconium added.

A somewhat different method of accounting for thermodynamic properties of intergrain gaps and internal space of nanograins was proposed;[21–23] it takes into consideration the difference in the free volume (ΔV) of the material at grain boundaries and in the bulk. The total enthalpy (H), entropy (S) and free energy (G) are expressed as follows

$$H = X_b H_b(\Delta V, T) + (1 - X_b) H_g(T) \quad (4)$$

$$S = X_b S_b(\Delta V, T) + (1 - X_b) S_g(T) \quad (5)$$

$$G = X_b G_b(\Delta V, T) + (1 - X_b) G_g(T) \quad (6)$$

where

$$\Delta V = \frac{V_b}{V_g} - 1$$

V_b and V_g are the unit cell volumes in intergrain gaps and inside the nanograins, respectively.

This expression for ΔV implies that there is excess volume in the grain boundaries due to disordered arrangement of atoms ($V_b > V_g$). The values of ΔV and thermodynamic quantities (ΔG, ΔH, heat capacity, the Debye temperature and so on) for intergrain gaps are selected taking into account experimental data (*e.g.*, see monograph [24]). This approach was applied to the analysis of thermal stability and phase transitions for a series of compounds in the Sm–Co system ($SmCo_5$, Sm_2Co_{17}, $SmCo_7$, *etc.*).[21–23,25,26] The calculated values of thermodynamic quantities for $SmCo_7$ as functions of temperature and grain size are shown in Fig. 6; as can be seen, the quantities increase at constant temperature with decreasing grain size, and this is especially pronounced when $d < 40$ nm (although this is less noticeable in the case of entropy).[23]

Among other theoretical studies, note the assessment of conditions required for spinodal decomposition in quasibinary Al_2O_3–ZrO_2 and TiN–SiN systems and analysis of

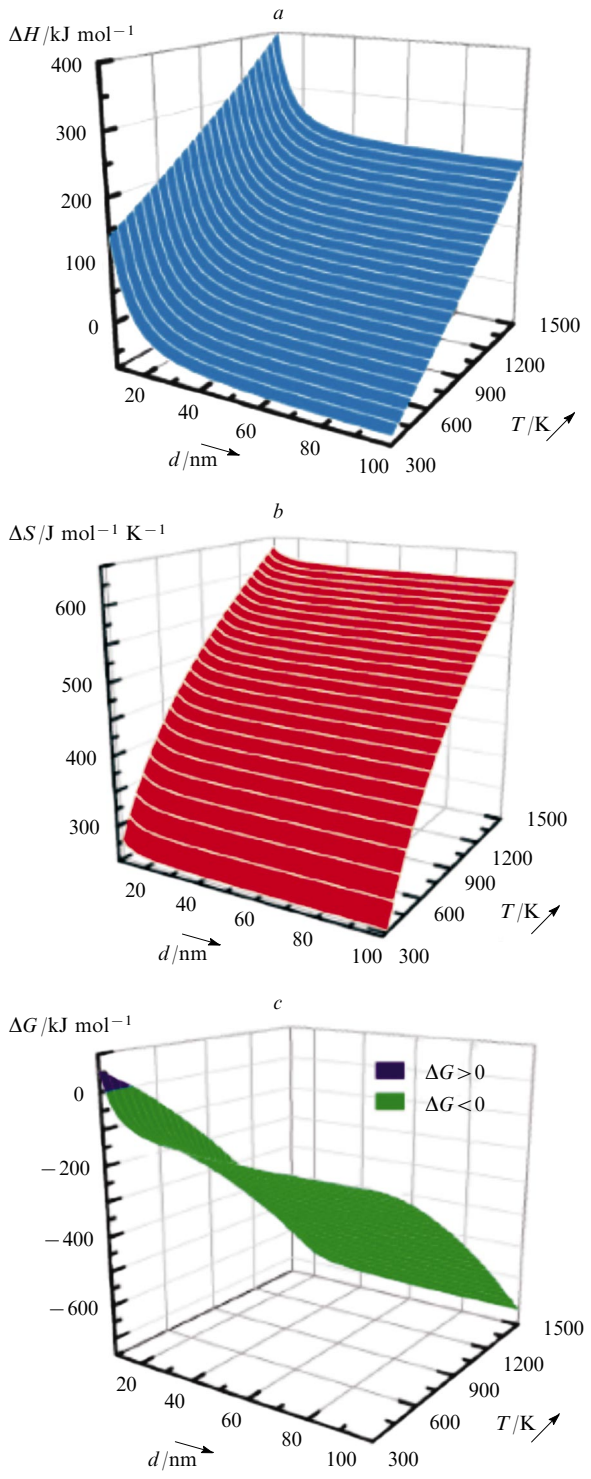


Figure 6. Enthalpy (*a*), entropy (*b*) and free energy (*c*) of $SmCo_7$ *vs.* grain size and temperature.[23]

behaviour of interfaces in multilayer TiN/SiN/TiN nanocomposites.[27–31] A combination of methods based on the thermodynamic approach and density functional theory calculations was used,[27–29] which enabled the authors to obtain not only thermodynamic characteristics, but also parameters of electronic and crystal structures and elastic constants. The calculations showed that the top of the spinodal and binodal decay dome for the metastable $TiN_{FCC}-SiN_{FCC}$ system is at the level of $\sim$3200 K, whereas the system has virtually two phases at $T < 1273$ K.[27] Some features of changes of the thermal stability of interfaces in various heterostructures formed by TiN/SiN and TiN/Si_3N_4 monolayers were revealed at temperatures between 0 and 1400 K using molecular dynamic calculations.[30, 31] In particular, it was noted that the thermal stability of cubic modification of SiN can be related to formation of vacancies in the silicon sublattice.[25] Unfortunately, the role of size effects was not analyzed in these studies.[27–31]

While noting the informativity and efficiency of calculations of thermodynamic properties of nanosystems (see Figs 5 and 6), one should dwell on applicability of classical thermodynamics to nanoscale objects. In Rusanov's opinion,[32] the conventional concepts of surface energy are quite applicable to nanoparticles of >10 nm size. If the nanoparticle size is <1 nm, virtually the whole nanoparticle (or nanolayer) may acquire the properties of a surface, which differ from the properties of the bulk phase, and a special approach is required in this case. The region of nanoparticle sizes between 1 and 10 nm is intermediate, and an analysis of the applicability is necessary in each particular case. Glezer[33] noticed another criterion for the loss of nanocrystallinity, namely, with the elimination of symmetry elements intrinsic to the crystal. The preservation of symmetry elements is considered to be reasonable down to a nanoparticle size comparable with the size of three coordination spheres. In the case of BCC and FCC lattices, the minimum size of crystallites is $\sim$0.5 (α-Fe) and 0.6 nm (Ni). Recently, the minimum nanoparticle size (predominantly in the liquid state) suitable for the application of classical thermodynamics was estimated.[34, 35] Taking into account spontaneous thermal fluctuations in droplets of $<41\,\lambda$ size (λ is the mean distance between molecules in a liquid), application of thermodynamic equations to these droplets is considered to be of low utility, while application of these equations to droplets of $>(90-100)\,\lambda$ size is strictly substantiated.[34] Thus, on the basis of the available data,[32–35] it is possible to conclude tentatively that the sizes of crystallite boundaries including the near-boundary regions roughly correspond to the lower limit of the particle size to which classical thermodynamics is applicable. However, the general problem of the thermodynamic description of the behaviour of grain boundaries in the consolidated nanomaterials remains unsolved and requires further theoretical and experimental research.

III. Experimental studies of high-temperature behaviour of nanomaterials

1. Studies of thermal stability

The thermal stability of nanocrystalline alloys based on copper, iron and nickel has been studied most comprehensively. The temperature dependences of grain growth in the Cu–Zr, Fe–Zr, Fe–Ni, Fe–Ta and Fe–Cr systems are shown in Fig. 7. These data indicate that alloying increases the thermal stability. The zirconium and tantalum additives have the most efficient influence on iron alloys. The calculated and experimentally obtained sizes of grains in the Cu–5 at.% Zr alloy in the temperature range of 300–700 °C (see Figs 5 and 7 and Table 2) differ by a factor of 4–10. Since an approximate model was used in

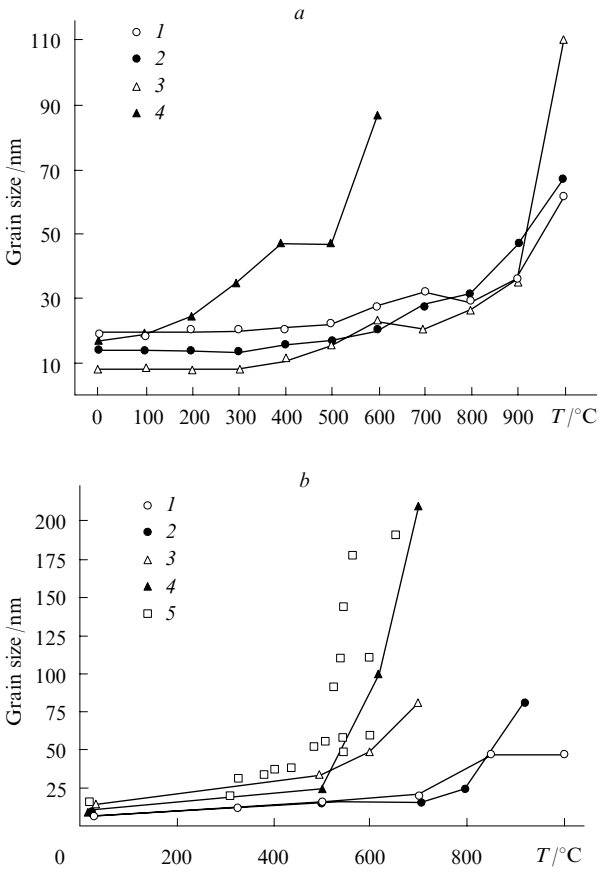


Figure 7. Effect of temperature on the grain size after annealing of copper (*a*) and iron (*b*) alloys for 1 h.[36,37]
(*a*) Cu–Zr alloy with zirconium content of 1 (*1*), 2 (*2*), 5 (*3*), 0 (pure copper) (*4*) at.%; (*b*) iron alloys containing 1 at.% of Zr (*1*), 1 at.% of Ta (*2*), 10 at.% of Cr (*3*), 1 at.% of Ni (*4*) and pure iron (*5*).

Table 2. Calculated and experimentally obtained grain sizes in annealed Cu–5 at.% Zr alloy.

Annealing temperature /°C	Grain size /nm	
	calculation [19]	experiment [37]
300	35	9
500	55	15
700	220	22

the theoretical study,[19] the results may be considered as satisfactory.

The predicted [17] nanocrystalline state of the W—Ti alloy (see Fig. 4) was confirmed for the W–20 at.% Ti powder with the initial nanograin size of 20 nm, which remained practically unchanged after annealing at 1100 °C for a week, whereas the size of nanograins in unalloyed tungsten was ~600 nm after the same treatment. The study of titanium distribution in the nanostructure showed that this alloy is heterogeneous with titanium content varying from 0 at.% to 50 at.%. Therefore, the thermal stability of the W–20 at.% Ti alloy is determined by not only the decrease in free energy, but also the formation of segregation inclusions and Zener pinning. A similar situation (*i.e.*, operation of two mechanisms) could also take place in the case of annealing of the Cu–5 at.% Zr alloy at 700 °C; the difference between the theoretical (only one mechanism was considered) and experimental results was the largest in this case (see Figs 5 and 7).

A comparison of the efficiencies of kinetic and thermodynamic approaches in consideration of the retardation of thermal growth of nanograins was reported by Koch *et al.*[38] For comparison of the experimental data obtained by different authors, the data were normalized against their melting points (T_m) in a homologous temperature scale. Only the data obtained with the use of transmission electron microscopy and X-ray diffraction analysis for annealed samples with grain sizes below 100 nm were included into consideration. The alloys based on Al, Mg, Cu and Fe with nanoinclusions such as Al_2O_3, AlN, ZrO_2 and Nb were found to be thermally stable at high homologous temperatures [up to $(0.75–0.85)\,T_m$]. Lower thermal stability [up to $(0.35–0.65)\,T_m$] was observed for Ni, Co, Fe, Y, RuAl and TiO_2 alloys containing W, P, Zr, Fe and Ca additives.

High thermal stability was found for copper-based alloys with tungsten and tantalum additives (10 at.%).[39,40] These alloys were prepared by high-energy cryogenic milling ($T = -196$ °C) of starting powders followed by pressing and sintering. The starting size of grains in Cu–W alloy was ~15 nm, and after annealing at 800 °C, it was ~60 nm.[39] The Cu–Ta alloys were studied in detail with the use of various methods, the major data are presented in Table 3. As can be seen, the thermal stability of these alloys is rather high. Note for comparison that microhardness of the Cu—10 at.% W alloy in the initial and annealed samples at 800 °C was ~3 and 2.6 GPa, respectively [39] (these figures are smaller than the value reported in the most recent study [40]).

Detailed discussion of the obtained results and different mechanisms responsible for thermal stability, including the effect of triple junctions, alloying, presence of inclusions and segregations, made it possible to conclude [40] that the observed high thermal stability of Cu—Ta alloys was due to formation and subsequent decomposition of tantalum segregations at grain boundaries, *i.e.*, due to combined action of both thermodynamic and kinetic mechanisms. The latter operates at high temperatures, being a result of decomposition of near-boundary layers with formation of inclusions (called nanoclusters by the authors [40]), which ensure retardation of nanograin growth at high temperatures. The results of molecular dynamic calculations and experimental studies of sample structures using transmission electron microscopy confirm this conclusion.[41]

Table 3. Changes in the nanostructure and microhardness of Cu—10 at.% Ta alloys after annealing for 4 h under hydrogen atmosphere.[40]

Annealing temperature /°C (see [a])	Grain size /nm		Microhardness /GPa
	Cu	Ta	
20 ($0.22T_m$) — initial state	6.7	6	4.8
540 ($0.6T_m$)	21 ± 4	22 ± 45	~3.6
770 ($0.77T_m$)	54 ± 9	37 ± 9	—
900 ($0.87T_m$)	111 ± 26	42.5 ± 25	3.4
1040 ($0.97T_m$)	167 ± 50	99 ± 99	2.6

[a] Homologous temperature.

Significant role of the kinetic mechanism (inhibitory action of nanoprecipitation) in the thermal stability was also noted in the study of Cu–Nb, Ni–Y and Fe–Zr nanoalloys.[42–44] At the same time, this effect was not observed for the Cu–Fe and Pd–Zr systems.[42,43]

It is noteworthy that the regularities of nanolayer decomposition and formation of nanoinclusions have not yet been adequately investigated, and the search for new thermally stable nanomaterials is based on the concepts of conventional material science concerning the manufacture of dispersion-strengthened systems with the use of various techniques. In particular, new grades of ferrite and ferrite–martensite steels are produced by powder technique (high-energy milling of the starting components and consolidation under nanostructure-preserving conditions).[5,45] The presence of oxide inclusions in the iron–chromium steels such as $Y_2Ti_2O_7$ and Y_2TiO_5 of 2–4 nm size, which are thermally stable and possess good adhesion to the matrix, is a prerequisite to thermal stability of the nanostructure of these steels and, hence, to the retention of their mechanical characteristics on exposure to radiation. These steels the radiation stability of which is determined by the presence of multiple grain boundaries, which absorb radiation defects, are the materials used for fuel element cans of fast-neutron reactors of new generation; thus, the available experimental data are encouraging.

It was proposed to apply severe plastic deformation such as torsion at 4 GPa to embed carbon nanotubes in copper nanocrystals.[46] This technique ensures the formation of materials with hardness of ~2.1 GPa (the hardness is ~0.7 GPa after annealing at 700 °C).

The results obtained for films and multilayer structures are also noteworthy (*e.g.*, see Refs 47–50). Substantial strength and plasticity of copper films with twin nanointerlayers (nanolamellae) has long been known (*e.g.*, see the monograph [1]), but their high thermal stability was revealed quite recently during studies of annealing effects.[47] As can be seen from Fig. 8, in contrast to nanograin growing, the width of twin interlayers, which determines the high hardness, changes very little, a significant hardness being retained even after annealing at 800 °C ($0.74\,T_m$); this characteristic is substantially superior to that of copper with usual nanocrystalline structure but inferior to that of the Cu—Ta alloy. It was also shown [47] that small-angle coherent boundaries between the lamellae have lower temperature susceptibility than large-angle boundaries, which are typical of conventional nanomaterials. The next step in this area was creation of bulk two-phase nanocomposites like Cu/Nb with the layer thickness of up to 10 nm, which are produced by multiple pack rolling. They have the interface $\{551\}\langle 111\rangle Cu||\{112\}\langle 111\rangle Nb$ and are characterized by the nanotwinning deformation.[48] After annealing at 500 °C, their hardness decreased by less than 1.5% (from 4.13 to 4.06 GPa); this index is the best among the indexes of known nanocomposites.

The studies of thermal stability of film samples revealed the role of nanoprecipitation in the grain growth retardation in three-phase Co—Cu—Ag alloys [49] and indicated that it is expedient to irradiate Cu—Nb—W alloys with krypton ions to promote formation of nanoprecipitates.[50]

The above discussion mainly concerned the thermal stability of metal-based nanomaterials. More examples of observations of nanograin growth in nanostructured oxides of aluminium, zirconium, titanium, tin and other metals can be found in earlier reviews.[51,52] The role of triple junctions in inhibition of grain growth in Y_2O_3 was analyzed in detail by Chokshi.[53]

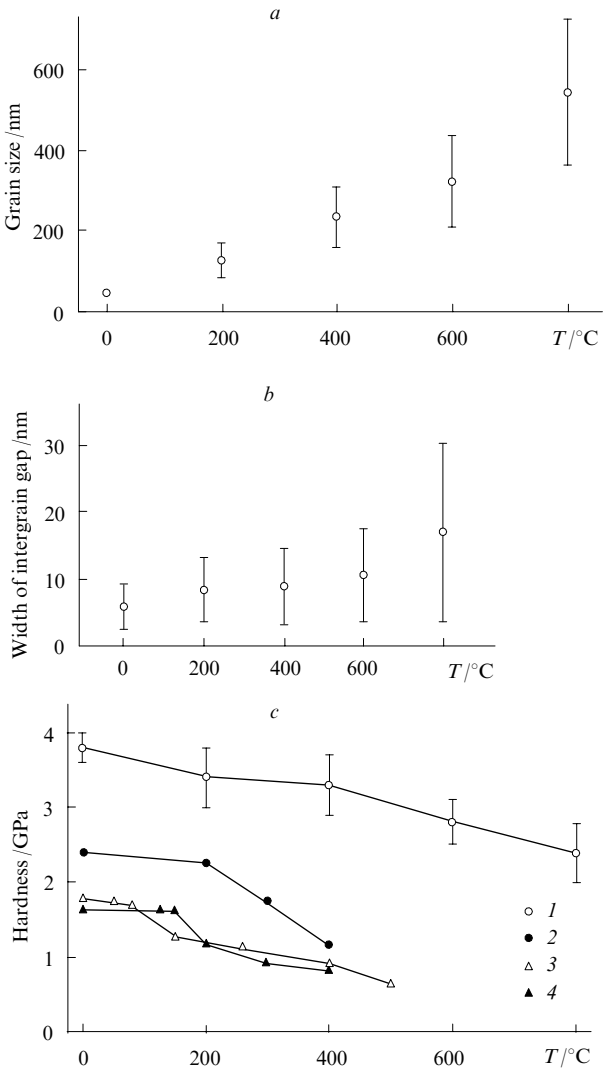


Figure 8. Effect of annealing temperature on the grain growth (*a*), width of nanolamellae (*b*) and hardness (*c*) of copper samples with different structure.[47]
(*c*) (*1*) Films with nanolamellae, (*2–4*) conventional samples with ultrafine-grained and nanocrystalline structures according to the data of different authors.

2. Abnormal grain growth

Abnormal grain growth (or secondary recrystallization) consisting in the formation of coarse grains, which absorb smaller ones, is well known for coarse crystalline materials and has long been studied (see, *e.g.*, the monograph [54]). In the case of nanomaterials, this phenomenon, which can occur not only upon heating but also at room temperature, can result in complete decay of the nanostructure and considerable deterioration of characteristics of the material. This determines the interest to study abnormal grain growth and also to develop methods for predicting and preventing this effect. During conventional grain growth, the grain size

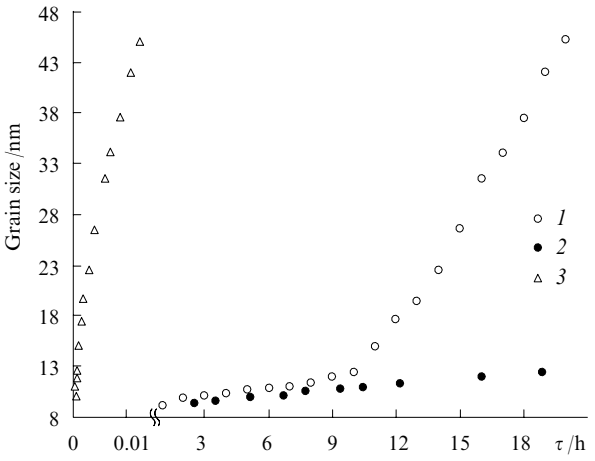


Figure 9. Kinetics of grain growth in nanocrystalline palladium ($T = 20$ °C).
(*1*) Experimental data;[56] (*2*) results of calculations with allowance for inhibition by triple junctions;[57] (*3*) results of calculations without allowance for inhibition by triple junctions.[57]

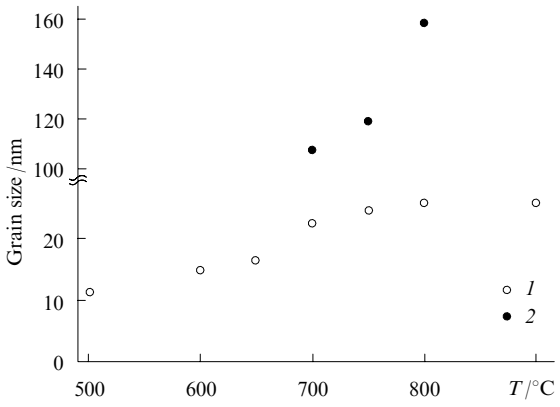


Figure 10. Temperature effect on grain growth in $Fe_{91}Ni_8Zr$ alloy.[62]
(*1*) α-phase; (*2*) γ-phase.

distribution remains predominantly lognormal; when abnormal grain growth occurs,[55] areas with large grains appear, and the distribution becomes bimodal (see the data on the increase in the mean square error of measurements with increasing temperature in Table 3).

Experimental data and results of theoretical simulations of grain growth kinetics in nanocrystalline palladium at room temperature are shown in Fig. 9. As can be seen, there is satisfactory agreement between the experimental[56] and theoretical[57] data before the abnormal grain growth starts (the growth lasted >9 h). However, the discrepancy between the data would be substantial if the inhibiting effect of triple and quadruple junctions was not taken into account. At the same time, neither the existence of a large number of junctions nor the presence of residual porosity (the initial grain sizes were ~ 5 nm, the porosity of the samples was 4%) or residual hydrogen (0.4 at.%), nitrogen (0.2 at.%) and oxygen (0.1 at.%) could prevent the abnormal growth, due to which the palladium nanostructure was transformed into a conventional microstructure with grain sizes of ~ 10 μm within ~ 2 months at room temperature.[56]

The phenomenon of abnormal grain growth at room (or elevated) temperature was experimentally observed for many nanomaterials based on copper,[40,58] nickel,[55,59,60] iron,[61,62] hard alloys (WC–Co)[63] and diamond[64] (see also references to earlier studies in monographs[1,4]), in particular, using transmission electron microscopy *in situ*.[40,59–61] It is noteworthy that the listed nanomaterials were synthesized using different methods such as pulsed electrodeposition,[55] pressing and sintering,[57,63] severe plastic deformation (torsion at 4.5 GPa) at liquid nitrogen temperature,[58] pulsed laser deposition,[59,60] intensive mechanical milling and mixing (mechanosynthesis),[40,61,62] sintering under high pressures ($T = 1400$ °C, $P = 6.8$ GPa).[64] Naturally, such variety of approaches affected the initial and final states of the research subjects. For instance, electron microscopy studies of nickel films *in situ* showed[59,60] that annealed samples contained numerous defects such as tetrahedral stacking faults and dislocation loops, and also low-energy twin boundaries. The revealed instability of copper nanostructure at room temperature led the authors[58] to conclusion that application of low-temperature plastic deformation has no prospects in manufacturing of nanomaterials. The study of thermal stability of the $Fe_{91}Ni_8Zr$ alloy *in situ* showed that abnormal grain growth starting above 700 °C is related to the formation of FCC crystals of the γ-phase (Fig. 10).[62]

Theoretical description of abnormal grain growth in nanomaterials was also attempted.[13,14,65–67] In accordance with the statistical model of temperature evolution of grain structure, which was developed earlier, the mobility, number and size of nanoinclusions, which inhibit growing of grains, are taken into account in the kinetics of grain growth. The analysis of data of numerical modelling indicated that the tendency to abnormal grain growth increases with increasing mobility of nanoinclusions, while the influence of their radius and number is non-monotonic. The calculated kinetic dependences[13] of aluminium grain size at

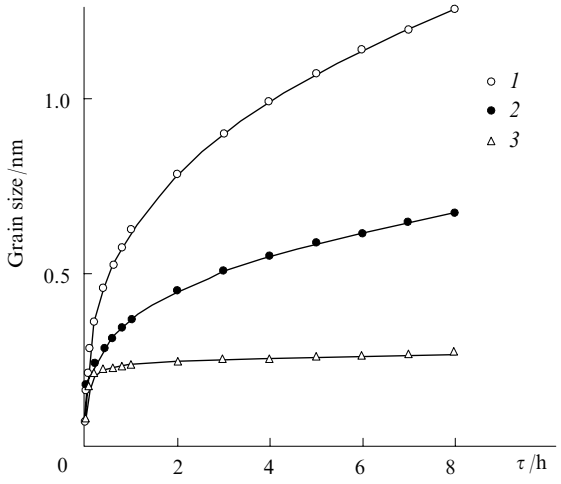


Figure 11. Kinetics of growth of aluminium grains at 400 °C for boundaries with mobility of 1 *M* (*1*), 0.1 *M* (*2*), 2×10^{-3} *M* (*3*).[13]

400 °C for different mobilities (M) of inclusions are shown in Fig. 11

$$M = \frac{(\delta D_s \Omega / kT)}{\pi r^4}$$

where δ is the width of particle/matrix interface, D_s is the surface diffusion coefficient, Ω is atomic volume, r is nanoinclusion radius (for the assumed[13] value of $M = 2 \times 10^{-4}$ cm^4 J^{-1} s^{-1}).

At the same time, many important aspects of abnormal grain growth in nanomaterials (the effect of initial nanograin size, number of defects and admixtures, the balance of thermodynamic and kinetic factors, the role of technique used, *etc.*) remain yet unexplored in detail either experimentally or theoretically.

3. Oxidation of nanomaterials

Contradictory data were obtained in the studies of interactions of nanomaterials with corrosive media.[1,4,6] In the general case, the presence of numerous interfaces (*i.e.*, areas with disordered structure) should promote corrosion. However the formation of protective surface films by diffusion (*i.e.*, surface passivation) could also be more active due to disordering, thus preventing propagation of corrosion. Simultaneous operation of these factors determines the result of interaction of nanomaterials with the surrounding media. This result is dependent on specific features of the nanostructure, including its thermal stability. The data on oxidation of nanomaterials based on some metals and refractory compounds are discussed below.

The kinetic dependences of oxidation of nano- and microcrystalline iron alloys and pure nickel with grains of different size are shown in Fig. 12. The researchers[68–70] paid special attention to preparation and certification of initial samples, which were obtained by mechanosynthesis followed by hot compaction and sintering (iron alloys)[68,69] or electrodeposition (pure nickel).[70] The grain size was controlled by annealing, whereas structural bimodality (simultaneous presence of nano- and micrograins)[68,69] was achieved by mixing powders with nano- and micrograins. As can be seen from Fig. 12 *a*, the transition to nanostructure or bimodal structure (nanograin and micrograin sizes of 58±4 nm and ~2 μm, respectively) for iron–chromium alloys (the concentrations are given in mass %) is accompanied by a pronounced decrease in the oxidation rates. Nanoalloys with 10 mass % Cr and microalloys with 20 mass % Cr are equally stable against oxidation. Due to presence of coarse grains in the nanocrystalline matrix, the structural bimodality substantially increases the plasticity of brittle materials but only slightly increases their oxidizability in comparison with nanoalloys (see also Refs 1 and 71).

Higher resistance of nanocrystalline Fe–10 mass % Cr alloys to oxidation in comparison with analogous coarse-grained alloys was demonstrated earlier.[72] However, the test duration used then was within 50 h; therefore, reinvestigation was undertaken[68,69] with the purpose to increase the test duration and to reveal the capabilities of bimodal alloys with high plasticity. When minor zirconium additives were introduced in the Fe–Cr–Ni alloys, nanostructure of the alloys remained unchanged upon prolonged exposures (see also Fig. 5 *a*). Using secondary ion mass spectrometry, it was found that chromium content in the surface layers of

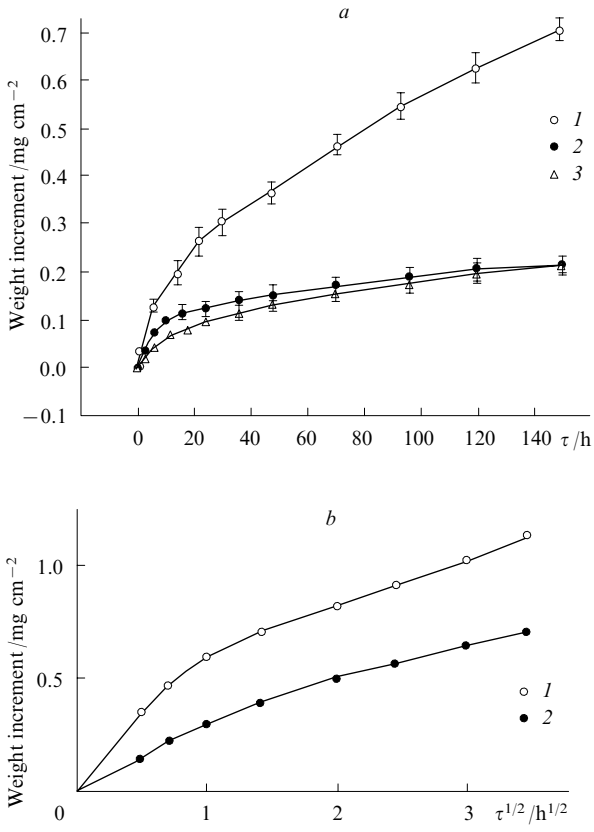


Figure 12. Kinetics of oxidation of Fe–Cr–Ni–Zr alloys (*a*)[68,69] and pure nickel (*b*).[70]
(*a*) Microcrystalline Fe–10 Cr–5 Ni alloy (*1*), Fe–10 Cr–5 Ni–2 Zr alloy with bimodal structure (*2*), nanocrystalline Fe–10 Cr–5 Ni–2 Zr alloy (*3*); (*b*) nanocrystalline samples with grain size ~28 nm (*1*), coarse-grained samples with grain size ~3.5 μm (*2*).

alloys with bimodal structure and nanostructure was higher than in the microcrystalline alloys due to enhanced diffusion mobility of chromium in nanograins. As a result, the formation of compact protective film of Cr_2O_3 decreased the rate of oxidation of bimodal alloys and nanoalloys.[68,69,72]

The opposite situation was observed for nickel (Fig. 12 *b*): nanocrystalline samples were oxidized more actively than coarse-grained ones, including the temperature range 800–900 °C.[70] The analysis of kinetic and diffusion data showed that the difference in behaviour of nanocrystalline and coarse-grained samples is related only to the initial stage of oxidation, *i.e.*, to deviation from known parabolic growth law, and is caused by more active formation of NiO islands on the nickel surface. The activation energy of oxide layer growth during the steady-state period was found to be practically the same for nanocrystalline and course-grained samples and equal to ~108 kJ mol^{-1}; this value coincides with the activation energy of grain boundary diffusion of nickel in NiO.[70]

A decrease in the oxidation rate at 600–800 °C (exposure for 60 min) was observed for technical-grade titanium with the decrease of grain size from 0.46 to 0.15 μm.[73] An increase in the oxidation resistance on going to the nanocrystalline state was reported for electrodeposited nickel

nanocomposites with nanoinclusions of chromium, aluminium [74] and zirconium,[75] and also for some alloys containing chromium, aluminium and silicon (Ni–Cr–Al, Cu–Ni–Cr, Fe–B–Si, Cr–Nb, *etc.*), although there are opposite (or ambiguous) observations, especially in the case of corrosion in inorganic acids (see references in reviews [6, 76]). The discrepancies in the assessments of stability of nanomaterials against corrosion have different reasons (the degree of nanocrystallinity of formed protective films, their composition, structure imperfection, coating continuity and formation rate, presence of segregations at interfaces, specific features of corrosive media, *etc.*).

Due to increase in the operating temperatures of cutting tools and friction assemblies, as well as coatings for aerospace applications, the interest in improving the oxidation resistance of refractory carbides, borides and nitrides is unabated (*e.g.*, see Refs 77–79). Nanostructured SiC coating with 150 nm thickness significantly reduces the oxidation of carbon fibres at 600 °C.[77] An analysis of behaviour of refractory coatings revealed the following materials for particular temperature ranges:[78]

— nanostructured coatings based on (Ti,Al)N, TiN–Si_3N_4 and (Ti,Al,Cr,Y)N and multilayer (Ti,Al)N/CrN films are stable up to 1000 °C;

— amorphous coatings based on Si–Ta–N, Si–Zr–N, Si–Al–N, Si–Ti–N and Si–Mo–N are stable up to 1500°C;

— complex amorphous Si–B–C–N compounds are characterized by high thermal stability up to 1700 °C.[80]

As can be seen, amorphous coatings significantly surpass nanocrystalline coatings; this can be attributed to the formation of cracks in the latter, which reduce their limiting characteristics. However, it is unclear what exposure duration to oxidative media was chosen to determine the above listed temperature ranges.

To protect composites such as carbon fibre/SiC, up to 50 μm-thick coatings $ZrB_2(HfB_2)$/SiC were studied;[79] the coatings were deposited by annealing of the slurry at 1200 °C. It was found that the residual porosity of these coatings is high, and their nanostructurization can be useful to decrease the porosity.

IV. Conclusion

As can be seen from the above discussion, many interesting experimental and theoretical results concerning the thermal stability of consolidated nanostructured materials have been obtained recently. The data indicating the possibility of estimation of thermodynamic properties of nanomaterials in regular solution approximation seem especially important. It seems also that the capabilities of prediction and practical implementation of increased thermal stability and microhardness and also other functional characteristics of practically important heat- and radiation-resistant and corrosion-proof metal-based nanomaterials are far from being exhausted. Nonetheless, detailed experimental testing and refinement of this approach remain to be performed, in particular, by extending these studies to oxide-, carbide- and boride-containing materials and other objects. High thermal stability has been revealed in experiments for nanostructured TiAlSiCN coatings annealed at temperatures up to 1300 °C.[81]

Thermal stability of carbon containing nanostructures in the form of graphene and nanotubes, an important class of nanomaterials, remains little studied. At the recent 11th International Conference 'Advanced Carbon Nano-Structures' (Saint Petersburg, July 1–5, 2013), among numerous reports, only one poster [82] was devoted to the study of degradation of carbon nanotubes as a basis of autoelectronic emission cathodes, *i.e.*, to the thermal stability of the nanotubes.

It is necessary to emphasize that the least investigated problem is abnormal grain growth, which can largely cancel out all the advantages of nanomaterials. Are all nanomaterials prone to abnormal grain growth, what are the conditions promoting it, can it be predicted and supressed? These issues remain unanswered and require profound studies.

The author is grateful to V V Klyucharev and S V Klyucharev for effective help in the work on this review. The review was prepared under financial support of the Russian Foundation for Basic Research (Project No. 13-03-01014) and the Division of Chemistry and Materials Science of the Russian Academy of Sciences (programme No. 8).

References

1. R A Andrievski *Osnovy Nanostrukturnogo Materialovedeniya. Vozmozhnosti i Problemy* (Foundations of Nanostructural Materials Science. Resources and Problems) (Moscow: BINOM. Laboratoriya Znanii, 2012)
2. R A Andrievski *Russ. Chem. Rev.* **71** 853 (2002)
3. I A Ovid'ko *Mater. Phys. Mech.* **8** 174 (2009) [*Fiz. Mekhan. Mater.* **8** 174 (2009)]
4. K Koch, I Ovid'ko, S Sil, S Veprek *Konstruktsionnye Nanokristallicheskie Materialy. Nauchnye Osnovy i Prilozheniya* (Structural Nanocrystalline Materials. Scientific Foundations and Applications) (Moscow: FIZMATLIT, 2012)
5. R A Andrievski *Nanotechnol. Russ.* **6** (5–6) 357 (2011) [*Ros. Nanotekhnol.* **6** (5–6) 34 (2011)]
6. R A Andrievski *Prot. Met. Phys. Chem. Surf.* **49** 528 (2013) [*Fizikokhim. Poverkhn. Zashch. Mater.* **49** 491 (2013)]
7. M Upmanyu, D J Srolovitz, A E Lobkovsky, J A Warren, W C Carter *Acta Mater.* **54** 1707 (2006)
8. N Bernstein *Acta Mater.* **56** 1106 (2008)
9. R Chaim *Scr. Mater.* **66** 269 (2012)
10. I Zizak, N Darowski, S Klaumünzer, G Schumacher, J W Gerlach, W Assmann *Nucl. Instrum. Methods Phys. Res., Sect. B* **267** 944 (2009)
11. V Yu Novikov *Mater. Lett.* **62** 2067 (2008)
12. B Zhao, G Gottstein, L S Shvindlerman *Acta Mater.* **59** 3510 (2011)
13. V Yu Novikov *Acta Mater.* **58** 3326 (2010)
14. V Yu Novikov *Mater. Lett.* **68** 413 (2012)
15. L Klinger, E Rabkin, L S Shvindlerman, G Gottstein *J. Mater. Sci.* **43** 5068 (2008)
16. J R Trelewicz, Ch A Schuh *Phys. Rev. B* **79** 094112 (2009)
17. T Chookajorn, H A Mordoch, Ch A Schuh *Science* **337** 951 (2012)
18. H Murdoch, Ch A Schuh *Acta Mater.* **61** 2121 (2013)
19. M Saber, H Kotan, C C Koch, R O Scattergood *J. Appl. Phys.* **113** 063515 (2013)
20. B S Bokshtein, M I Mendelev *Kratkii Kurs Fizicheskoi Khimii* (Short Course on Physical Chemistry) (Moscow: CheRo, 2001)
21. W W Hu, X Y Song, E D Li, J Wei, J X Zhang *J. Appl. Phys.* **105** 104310 (2009)
22. W Hu, X Song, N Lu, C Huang *Acta Mater.* **58** 396 (2010)
23. W Hu, X Song, Z Zhang *Appl. Phys. Lett.* **97** 181911 (2010)

24. R A Andrievski, A V Ragulya *Nanostrukturnye Materialy* (Nanostructured Materials) (Moscow: Akademiya, 2005)
25. W Hu, X Song, N Lu, M Seyring, M Rettenmayr *Nanoscale* **1** 238 (2009)
26. W W Hu, X Y Song, Z X Zhang *NANO: Brief Rep. Rev.* **7** 125012 (2012)
27. R F Zhang, S Veprek *Thin Solid Films* **516** 2264 (2008)
28. S H Sheng, S Veprek *Acta Mater.* **59** 297 (2011)
29. S H Sheng, R F Zhang, S Veprek *Acta Mater.* **59** 3498 (2011)
30. V I Ivashchenko, S Veprek, P E A Turchi, V I Shevchenko *Phys. Rev. B* **85** 195408 (2012)
31. V I Ivashchenko, S Veprek, P E A Turchi, V I Shevchenko *Phys. Rev. B* **86** 014110 (2012)
32. A I Rusanov *Russ. J. Gen. Chem.* **72** 495 (2002) [*Zh. Obshch. Khim.* **72** 532 (2002)]
33. A M Glezer *Ros. Khim. Zh.* **46** (5) 50 (2002) [a]
34. Yu K Tovbin *Russ. J. Phys. Chem. A* **86** 1356 (2012) [*Zh. Fiz. Khim.* **86** 1461 (2012)]
35. V A Babuk, A D Zelikov, R M Salimullin *Techn. Phys.* **58** 151 (2013) [*Zh. Tekh. Fiz.* **83** (2) 1 (2013)]
36. K A Darling, B K Vanleeuwen, J E Semones, C C Koch, R O Scattergood, L J Kecskes *Mater. Sci. Eng., A* **528** 4365 (2011)
37. M A Atwater, R O Scattergood, C C Koch *Mater. Sci. Eng., A* **559** 250 (2013)
38. C C Koch, R O Scattergood, M Saber, H Kotan *J. Mater. Res.* **28** 1785 (2013)
39. M A Atwater, D Roy, K A Darling, B G Butler, R O Scattergood, C C Koch *Mater. Sci. Eng., A* **558** 226 (2012)
40. K A Darling, A J Roberts, Y Mishin, S N Mathaudhu, L J Kecskes *J. Alloys Compd.* **573** 142 (2013)
41. T Frolov, K A Darling, L J Kecskes, Y Mishin *Acta Mater.* **60** 2158 (2012)
42. S Özerinç, K Tai, N Q Vo, P Bellon, R S Averback, W P King *Scr. Mater.* **67** 720 (2012)
43. C C Koch, R O Scattergood, B K Van Leeuwen, K A Darling *Mater. Sci. Forum* **715 – 716** 323 (2012)
44. K A Darling, L J Kecskes, M A Atwater, C C Koch *J. Mater. Res.* **28** 1813 (2013)
45. X L Wang, C T Liu, U Keiderling, A D Stoica, L Yang, M K Miller, C L Fu, D Ma, K An *J. Alloys Compd.* **529** 96 (2012)
46. P Jenei, J Gubiecza, E Y Yoon, H S Rim, J L Lábár *Composites, Part A* **51** 71 (2013)
47. O Anderoglu, A Misra, H Wang, X Zhang *J. Appl. Phys.* **103** 094322 (2008)
48. Sh Zheng, I J Beyerlein, J S Carpenter, K Kang, J Wang, W Han, N A Mara *Nat. Commun.* **4** 1696 (2013)
49. Y Chen, Y Liu, F Khatkhatay, C Sun, H Wang, X Zhang *Scr. Mater.* **67** 177 (2012)
50. X Zhang, J Wen, P Bellon, R S Avarback *Acta Mater.* **61** 2004 (2013)
51. A Gupta, S Sharma M R Joshi, P Agrawal, K Balani *Mater. Sci. Forum* **653** 87 (2010)
52. R H R Castro *Mater. Lett.* **96** 45 (2013)
53. A H Chokshi *Scr. Mater.* **59** 726 (2008)
54. S S Gorelik, S V Dobatkin, L M Kaputkina *Rekristallizatsiya Metallov i Splavov* (Recrystallization of Metals and Alloys) (Moscow: Moscow Institute of Steel and Alloys, 2005)
55. L Cheng, G D Hibbard *Mater. Sci. Eng., A* **492** 128 (2008)
56. M Ames, J Markmann, R Karos, A Michels, A Tschöpe, R Birringer *Acta Mater.* **56** 4255 (2008)
57. G Gottstein, L S Shvindlerman, B Zhao *Scr. Mater.* **62** 914 (2010)
58. T Konkova, S Mironov, A Korznikov, S L Semiatin *Scr. Mater.* **63** 921 (2010)
59. K Hattar, D M Follstaedt, J A Knapp, I M Robertson *Acta Mater.* **56** 794 (2008)
60. Kacher, I M Robertson, M Nowell, J Knapp, K Hattar *Mater. Sci. Eng., A* **528** 1628 (2011)
61. H Paul, C E Krill *Scr. Mater.* **65** 5 (2011)
62. H Kotan, K A Darling, M,Saber, R O Scattergood, C C Koch *J. Mater. Sci.* **48** 2251 (2013)
63. K Mannesson, J Jeppsson, A Borgenstam, J Ágren *Acta Mater.* **59** 1912 (2011)
64. A McKie, M Herrmann, I Sigalas, K Sempf, R Nilen *Int. J. Ref. Met. Hard Mater.* **41** 66 (2013)
65. V Yu Novikov *Mater. Lett.* **65** 2618 (2011)
66. V Yu Novikov *Int. J. Mater. Res.* (4) 446 (2011)
67. V Yu Novikov *Mater. Lett.* **84** 136 (2012)
68. B V Mahesh, B K Singh Raman, C C Koch *J. Mater. Sci.* **47** 7735 (2012)
69. B V Mahesh, B K Singh Raman, R O Scattergood, C C Koch *Mater. Sci. Eng., A* **574** 235 (2013)
70. A M Rashidi *Surf. Coat. Technol.* **205** 4117 (2011)
71. R A Andrievski, A M Glezer *Physics-Uspekhi* **52** 315 (2009) [*Usp. Fiz. Nauk* **179** 337 (2009)]
72. R K Gupta, R K Singh Raman, S S Koch *J. Mater. Sci.* **45** 4884 (2010)
73. A V Korshunov, A P Il'in A I Lotkov, I V Rotochka, T P Morozova, O N Lykova *Perspekt. Mater.* (4) 5 (2012)
74. X Peng *Nanoscale* **2** 262 (2010)
75. X Y Zhang, M H Shi, C Li, N E Liu, Y M Wei *Mater. Sci. Eng., A* **448** 259 (2007)
76. R K Gupta, in *Corrosion Resistance* (Ed. M Shih) (Vienna: InTech, 2012)
77. P C Kang, G Q Chen, B Zhang, G H Wu, S Mula, C C Koch *Surf. Coat. Technol.* **206** 305 (2011)
78. J Musil *Surf. Coat. Technol.* **207** 50 (2012)
79. X Yang, L Wei, W Song, Zh Bi-Feng, Ch Zhao-Hui *Composites, Part B* **45** 1391 (2013)
80. S H Lee, M Weinmann *Acta Mater.* **57** 4374 (2009)
81. D V Shtansky, K A Kutsov, Ph V Kiryukhantsev-Korneev, A N Sheveyko *Surf. Coat. Technol.* **206** 4830 (2012)
82. A V Eletskii, in *Abstracts of the 11th International Conference Advanced Carbon Nano-structures. ACNS'2013, St Petersburg, 2013* Poster P2.06

[a] — *Mendeleev Chem. J. (Engl. Transl.)*